PAPER

Check for updates

Polycaprolactone composite films infused with hyperbranched polyester/reduced graphene oxide: influence on biodegradability, gas/water transport and antimicrobial properties for sustainable packaging

Ahmed F. Ghanem,[a] Mohamed A. Yassin,[ab] Raphael Cosquer,[c] Fabrice Gouanvé,[c] Eliane Espuche[c] and Mona H. Abdel Rehim [ID] *[a]

Biodegradable polymers have gained great interest as ecofriendly packaging materials. However, addition of suitable fillers to the polymer matrix enhances their barrier and mechanical properties besides gaining new features such as bactericidal activity. This work deals with investigation of mechanical, gas/water transport properties and biodegradability performance of films based on polycaprolactone (PCL) reinforced by 1wt% of reduced graphene oxide (RGO) or modified graphene (mRG). To achieve this goal, nanosheets of RGO were firstly prepared then their surfaces were modified through *in situ* polymerization of hyperbranched polyester (PES) to obtain mRG. Then PCL was loaded with both fillers, and the nanocomposite films were prepared by a casting technique. Studying of the thermal properties of the films showed that the addition of RGO or mRG had no influence on the crystallinity of the PCL matrix. Although the mechanical characteristics of the PCL did not change when either filler was added, there was an increase in permeability and diffusivity in the presence of the fillers regardless of their composition. Nevertheless, the nanocomposites demonstrated antimicrobial properties against *S. aureus* and *E. coli* as models for Gram-positive and Gram-negative bacteria, respectively. The biodegradability test performed on the prepared film PCL, and those containing 1% of the filler, PCL/RGO, and PCL/mRG, emphasized that the film degradation became pronounced after three months for all samples.

Introduction

The recent accelerated ecological issues due to expanding utilization of plastics have increased researchers' interest in finding alternatives for synthetic polymers. Biodegradable polyesters are a class of macromolecules that can be degraded under special conditions in the presence of bacteria. They are classified into natural biodegradable polymers such as polylactic acid (PLA) and synthetic ones *e.g.* polycaprolactone (PCL) and polybutylene succinate (PBS). The pronounced increase in the synthesis of bio-based polymers using different techniques could be noticed in the last decade promoted by raising ecological concerns.[1–3] PCL is a semi-crystalline polymer that is mostly prepared from petroleum-based monomers by a ring-opining polymerization technique among other methods.[4] Its low glass transition temperature and melting point enable its mechanical processing. However, the addition of nanomaterials to PCL overcome its low thermal stability and degradation rate and enhances its gas and water vapor barrier properties. Moreover, the newly obtained nanocomposites can impart new properties such as antibacterial activity.[5]

Graphene (G) nanosheets[6] is characterized by its versatile properties that facilitate its application as a functional additive.[7] Nevertheless, surface modification of graphene is generally required to reduce restacking and improve its dispersion in the polymer matrix.[7] This can be attained either by a covalent approach or a non-covalent approach.[8,9] Grafting of graphene oxide (GO) by a macromolecule is found to increase its solubility in solvents and exfoliation of graphene in the polymeric matrix.[8,10] Modification of GO with polyvinyl imidazole and an ionic liquid to prepare CO_2 scavenger was studied.[10] The results revealed that surface functionalization of GO fostered the selective capture of CO_2. Blending of polymers with GO grafted with hyperbranched polymer (hbp) to attain high-performance composite[11] or increasing barrier properties of the formed material was investigated.[12,13]

[a]Packing and Packaging Materials Department, National Research Centre, Giza, Egypt. E-mail: monaabdelrehim23@gmail.com

[b]Advanced Materials and Nanotechnology Lab., Center of Excellence, National Research Centre, Giza, Egypt

[c]UMR CNRS 5223, Ingénierie des Matériaux Polymères, Université Claude Bernard Lyon 1, 69622 Villeurbanne Cedex, France

Incorporation of PCL with G to obtain nanocomposite of enhanced mechanical or electrical properties has found interest.[14–17] Sayyar et al. studied nanocomposites based on covalently linked PCL to graphene.[18] It was demonstrated that high graphene dispersion led to a composite of improved mechanical and electrical conductivity as well as good biocompatibility. An interesting study described the fabrication of robust and flexible multilayer 3D printed graphene/polycaprolactone composite electrodes that potentially serve as a conductive-biodegradable scaffold for electrical stimulation in promoting tissue formation for regenerative medicine.[19] Preparation of nanocomposites based on PCL and modified reduced graphene oxide (mRGO) has been studied lately.[20] The obtained films showed improvements in ductility, stiffness, and strength. Examining the kinetics of water sorption revealed a decline in the diffusion coefficient. Additionally, the barrier qualities improved with increased gas and water permeability. Additionally, biodegradability of the films based on the obtained nanocomposite demonstrated more and larger holes compared with the neat PCL film indicating the enhancement of PCL biodegradability by incorporation of RGO or mRGO. These results are aligned with those reported by Sánchez-González et al. who studied the in vitro hydrolytic degradation of PCL/RGO bio-scaffold.[21] Moreover, the results confirmed that the incorporation of RGO not only reduced the mechanical stability of the nanocomposite scaffold over the degradation times but also accelerated its degradation rate.

This work describes the in situ surface modification of RGO by hyperbranched polyester (PES) to facilitate its dispersion in PCL matrix. The chemical structure of the prepared nanocomposites was thoroughly studied before insertion in PCL. Thermal stability, mechanical, water, and gas transport properties of films based on PCL/mRG composites were studied. Investigation of antibacterial and biodegradation of the fabricated films was carried out as well.

Experimental part

Materials

4,4-Bis(4-hydroxyphenyl)valeric acid, HVA, (95%), sulfuric acid (99.9%), N,N-dicyclohexylcarbodiimide (DCC, 99%), and dried dimethylformamide (DMF, 99.9%) were bought from Sigma Aldrich, USA. 4-(Dimethylamino) pyridine (DMAP, 99%), p-toluene sulfonic acid monohydrate (TSA, 98%) are products of Merck. Graphite powder (99.9%) and tetrahydrofurane (THF, 99%) were supplied from Fisher Scientific-UK. Potassium permanganate (KMnO$_4$, 99%) and hydrogen peroxide (H$_2$O$_2$, 30%) were purchased from Bio Basic Inc.-Canada and Carl Roth GmbH-Germany, respectively. Sodium nitrate (NaNO$_3$, 99.99%) and hydrazine hydrate (NH$_2$NH$_2$, 99%) were provided by Sd Fine-CHEM limited-India. Commercial polycaprolactone pellets (PCL, average $\bar{M}_n$ = 80 000 g mol^{-1}) used in this study were supplied by Sigma Aldrich, Europe.

Methods

Synthesis of reduced graphene oxide (RGO). Graphene oxide (GO) was initially prepared using Hummers' method.[22] Here, 5 g of graphite powder was dispersed in a cooled solution of sodium nitrate (NaNO$_3$) dissolved in concentrated sulfuric acid. Then, 30 g of potassium permanganate (KMnO$_4$) was added to the mixture in order to oxidize graphite into graphene oxide (GO) and the temperature was kept at 30 °C. After 3 h, a liter of distilled water was carefully poured into the reaction vessel and the temperature was raised up to 98 °C for 30 min. After that, H$_2$O$_2$ (50 mL) was added dropwise to the mixture over 5 min and left for cooling on stand. The resultant suspension was filtered out, washed well, and dried. To obtain reduced graphene oxide, a dispersion of GO was sonicated for 30 min and then 50 μL of hydrazine (NH$_2$NH$_2$) was added and heated in the domestic microwave (1000 W) for 3 minutes. Finally, the obtained flakes of the reduced graphene oxide were filtered out, washed, and dried overnight under vacuum.

Surface modification of RGO nanosheets (mRG). The prepared RGO was in situ modified with hyperbranched polyester as follows: 10 wt% of RGO was sonicated in 15 mL DMF for 1 h using tip sonicator (100 Hz). Then, 4,4-bis(4-hydroxyphenyl) valeric acid (3 g) was added and the whole mixture was vigorously stirred in N$_2$ atmosphere. After 72 h, 0.5 g of 4-dimethylaminopyridinium 4-toluenesulfonate (DPTS), as a catalyst,[23] was added to the previous dispersed solution and left under stirring. After 30 min, 3 g of dicyclohexylcarbodiimide (DCC) was slowly added and the mixture was stirred at room temperature for 24 h. After that, the dispersed solution was filtered out and carefully washed with hot DMF for several times followed by distilled water to remove the urea derivative byproduct. Finally, the modified reduced graphene oxide nanosheets (mRG) were collected and dried at 60 °C under vacuum overnight.

Preparation of polycaprolactone composite films. Neat polycaprolactone film (PCL), PCL composite film containing RGO (PCL/RGO) and PCL composite film containing mRG (PCL/mRG) were fabricated using casting method. To prepare the casting solution, 1 wt% of mRG or RGO (based on the weight of PCL) were individually dispersed in 20 mL of THF. After 72 h, 2 g of PCL was added to the dispersed solution and the whole mixture was left under vigorous stirring for further 72 h. Finally, the solution was poured in a clean glass Petri dish and left on stand for drying. After 24 h, the free-standing films were obtained by peeling off from the glass dish.

Techniques

Morphology and structure analysis. Chemical structure of the prepared samples was analyzed with Vertex 80v Fourier transform infrared (FTIR) spectrophotometer, Bruker. The samples were heated at 80 °C under vacuum for 3 h before analysis. ^{1}H-NMR spectra were acquired on JEOL-ECA 500 MHz spectrometer in DMSO at 25 °C with tetramethylsilane (TMS) as internal standard. Raman spectra for the prepared powder samples were collected at laser wavelength 532 nm and laser power 0.10 MW at 25 °C using Raman Spectroscopy, Bruker Optics, Ettlingen (Germany). Elemental analysis of the prepared polymers and nanocomposites was studied by X-ray photoelectron spectroscopy (XPS). The results were collected on K-

ALPHA (Thermo Fisher Scientific, USA) with monochromatic X-ray Al K-alpha radiation −10 to 1350 eV spot size 400 micro mat pressures 10^{-9} mbar with full spectrum pass energy 200 eV and at narrow spectrum 50 eV. The surface morphology was investigated with transmission electron microscope (TEM, JEOL JEM-1230) at 120 kV. Scanning electron microscope (SEM) images for powder and film samples were taken using JEOL-SEM with acceleration voltage of 80 kV. Time of exposure was short and the maximum magnification was 2000× to avoid the deformation of specimen. The molecular weights of the prepared polymer samples were determined using PL-GPC 220 with DRI-detection (UK/Agilent, USA) coupled to multi-angle static light scattering (MALLS-detector Helleos II, Wyatt Technologies Corp., USA).

Thermal analysis. Differential scanning calorimetry (DSC) analysis was performed with TA Instruments (DSC QA200 New Castle, Delaware, United States) in which 10–15 mg of sample was placed in hermetic pan. A heating rate of 10 °C min^{-1} was used in temperature range of −80 to 150 °C followed by a cooling from 150 to −80 °C at the same rate. The values of glass transition temperature (T_g) were taken at the midpoint of the specific heat capacity (C_p) curve. The crystalline index of PCL was calculated from the melting enthalpy according to the following equation:

$$X_c\ (\%) = \frac{\Delta H_m}{\Delta H_m^0 \times \varphi_w} \times 100$$

where φ_w is the mass fraction of PCL in the film, ΔH_m is the melting enthalpy of the sample, ΔH_m^0 is the extrapolated value of the enthalpy corresponding to the melting of 100% crystalline pure PCL, which is taken at 139 J g^{-1}.[24,25]

Tensile tests. Criterion (MTS Systems, Créteil, France) tensile testing machine equipped with a 500 N load cell was used to perform uniaxial tensile tests for neat PCL and nanocomposite films. Tests were carried out at 23 °C on H3 type tensile specimens. The crosshead speed was adjusted to 20 mm min^{-1} and the gauge length at 10 mm. Values of tensile modulus (E), yield stress (σ_y), yield strain (ε_y), breaking stress (σ_b) and strain at break (ε_b) were determined from the stress–strain curve. The reported values of the mechanical characteristics were the arithmetic mean of at least seven different specimens.

Water contact angle measurements. Water dynamic contact angles were determined for the prepared films with Dataphysics-OCA 25 instrument. Particularly, a drop of water was deposited on the surface of 1×1 cm^2 piece of film and the picture was taken by Dataphysics-OCA 25 instrument. The values of contact angle were calculated using SCA20-software. The results are the average value of triplicate measurements.

Water sorption. Water sorption isotherms of the different films were determined at 25 °C by using the dynamic vapor sorption analyzer, DVS Advantage (London, United Kingdom). Each sample was pre-dried in the DVS Advantage by exposure to dry nitrogen until the equilibrated dry mass was obtained (m_0). A partial pressure of vapor (p) was then established within the apparatus by mixing controlled amounts of dry and saturated nitrogen and the mass of the sample (m_t) was followed as a function of time. The mass of the sample at equilibrium (m_{eq})

was considered to be reached when changes in mass with time (dm/dt) were lower than $2 \times 10^{-4}\%$ min^{-1} for at least 5 min. Then, vapor pressure was increased in suitable activity up to 0.9 by step of 0.1. The value of the mass gain at equilibrium (M) defined as $(m_{eq} - m_0)/m_0$ for each water activity (a_w) allowed to plot the water sorption isotherm for each sample.

The sorption rate was also estimated at each water activity by applying Fick's diffusion law. Considering the film thickness (L), the water diffusion coefficient (D) was calculated for the short time $\frac{m_{\text{water}\ t}}{m_{\text{water}\ eq}}$ according to the following equation:

$$\frac{m_{\text{water}\ t}}{m_{\text{water}\ eq}} = \frac{4}{L}\left(\frac{Dt}{\pi}\right)^{0.5}$$

where; $m_{\text{water}\ t}$ is the mass of water sorbed as a function of the time, $m_{\text{water}\ eq}$ is the mass of water sorbed at equilibrium for a given water activity and t the time. The precision on the values of the water mass gain at equilibrium and values of the diffusion coefficient was estimated to be better than 5%.

Water permeability. Water permeability measurements were performed on 5 cm^2 samples at 23 °C for a water activity equals to 1. MOCON PERMATRAN W 3/33 (Minneapolis, MN, United States) equipped with an infrared sensor was used for these measurements. Prior to the test, specimens were conditioned in nitrogen inside the unit for at least 12 h. Then, water vapor was introduced in the upstream compartment of the test cell. The water molecules transferred through the film were conducted by nitrogen carrier gas to the infrared sensor. The water permeability coefficient (P_{H_2O}) was calculated considering the following equation:

$$P_{H_2O} = \frac{J_{st_{H_2O}}L}{\Delta p}$$

where; L is the thickness of the film, $J_{st_{H_2O}}$ is the water stationary flux, and Δp (=2.377 cmHg) is the difference of the pressure between the upstream and the downstream compartments of the permeation cell. The values of P_{H_2O} were expressed in barrer (1 barrer = 10^{10} cm$_{STP}^3$ cm cm^2 s^{-1} cmHg^{-1} = 3.36×10^{-16} mol m^{-1} m^{-2} s^{-1} Pa^{-1}). The precision on the obtained values was estimated to be better than 5%

Gas permeability. Gas permeation properties were determined on films of effective area 3 cm^2. Carbon dioxide was used as permeant molecules. The gas permeation cell consisted of two compartments separated by the studied sample film. The temperature of the cell was set at 20 °C. A preliminary high vacuum desorption was realized on the both sides of the film to ensure that the static vacuum pressure changes in the downstream compartment were smaller than the pressure changes due to the gas diffusion. Then, the upstream side was provided with the gas test at pressure of 3 bars. The increased pressure in the downstream compartment was recorded as a function of time with a Datametrics pressure sensor. A steady-state line was obtained after a transitory state. The permeability coefficient, P, expressed in barrer unit was calculated from the slope of the steady state line. The precision on the values of the permeability coefficient was estimated to be better than 5%.

Antimicrobial and biodegradability tests

The antimicrobial activity for the prepared samples was tested against Gram-positive, *Staphylococcus aureus* (*S. aureus*), and Gram-negative bacteria, *Escherichia coli* (*E. coli*) using shack-flask method. The biodegradability test was carried out by burying strips of certain weights samples in soil according to a previously reported method but for 3 months.[26] The tensile strength was measured before and after the biodegradation test.
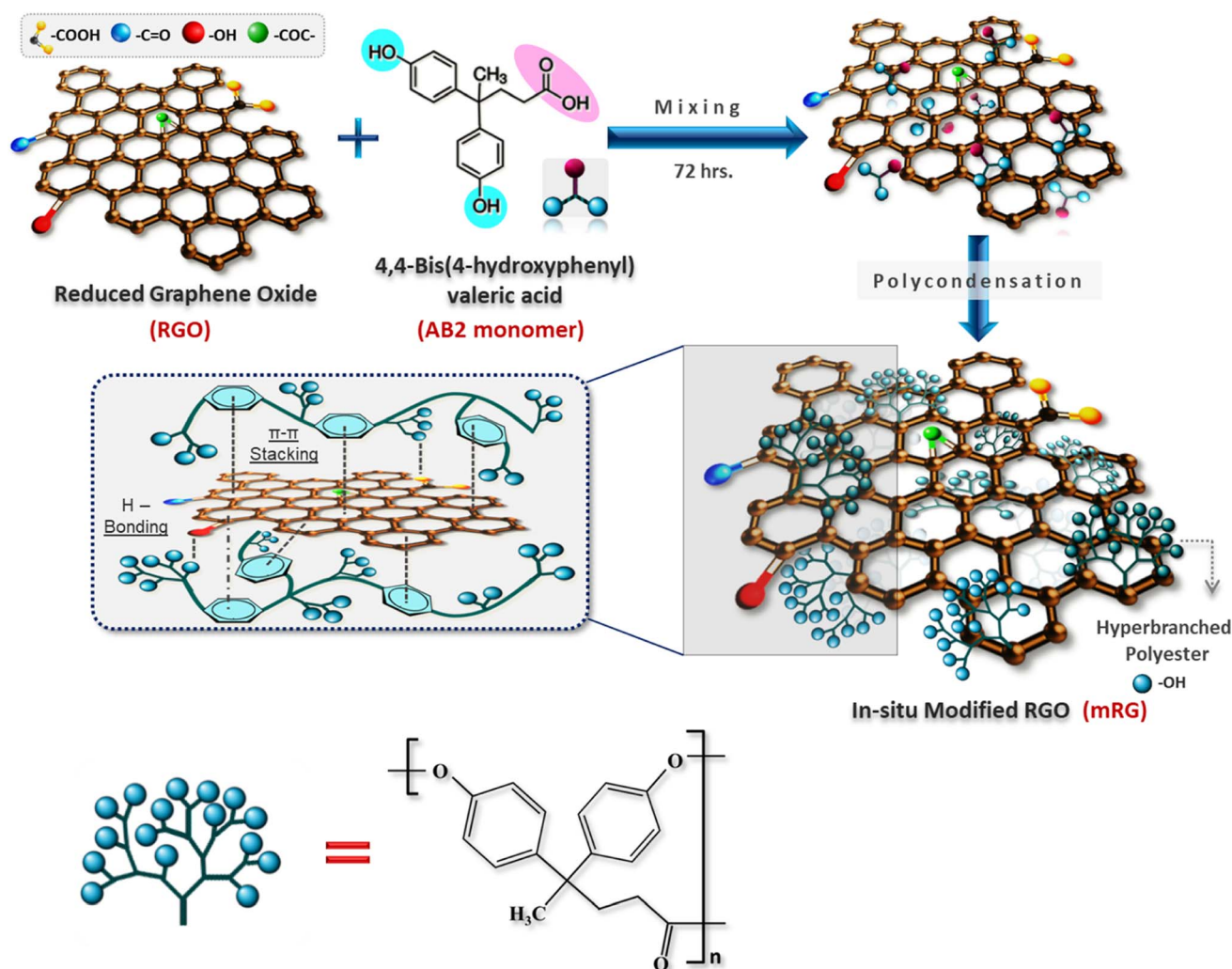
Results and discussion

Filler modification

Hyperbranched polyester (PES) was prepared in presence of RGO nanosheets (Scheme 1). The surface modified RGO nanosheets with PES (mRG) were separated *via* filtration. To confirm the polymerization step, the freely soluble PES was analyzed using ¹HNMR and the calculated degree of branching (DB) was found to be 58.5%. The GPC result showed that the freely soluble PES possesses molecular weight M_w of about 9400 g mol⁻¹ and dispersity (Đ) = 4.8.

The structure of hyperbranched polyester-modified reduced graphene oxide (mRG) was investigated by FTIR as shown in Fig. 1. The spectrum of mRG exhibits the main characteristic peaks of the hyperbranched polyester at ~3330 cm⁻¹ (–OH), 2900 cm⁻¹ (aliphatic –CH) in addition to stretching and bending vibrations of aromatic C=C at 1620 cm⁻¹ and 829 cm⁻¹, respectively.[26] Indeed, the spectrum of mRG displayed that the peaks corresponding to the aromatic rings in PES are blue-shifted (~15 cm⁻¹) which is likely due to the π–π interaction between the phenyl rings present in the entire structure of PES and graphene' surface.[7,27]

Raman spectra of both RGO and mRG showed two distinguished peaks which corresponded to the D and G bands in graphene, at the identical locations, 1334 and 1584 cm⁻¹, respectively (Fig. 2). One can observe that the ID/IG ratio of RGO and mRG were 1.16 and 1.17, respectively. This ratio provides information about the degree of disorder or defects in the graphene structure. The nearly equal ratios indicate that the modification step did not cause extra defects in the graphene structure.

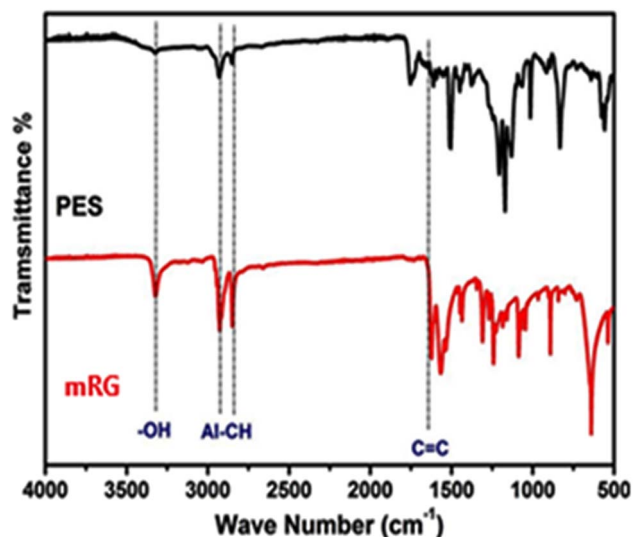**Scheme 1** Representation for the *in situ* polymerization reaction to achieve mRG.

Fig. 1 FTIR spectra of pure hyperbranched polyester (PES) and reduced graphene oxide modified with PES (mRG).
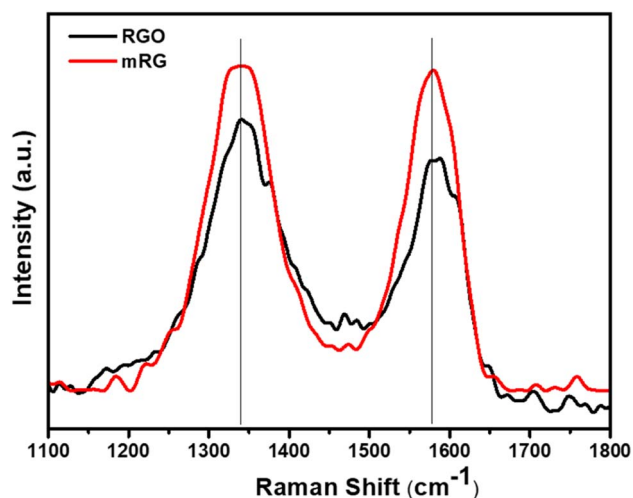

Fig. 2 Raman spectra of pure reduced graphene oxide (RGO) and its modified form (mRG).

RGO and mRG were subjected to morphological investigations using TEM, as illustrated in Fig. 3A. RGO appeared as wrinkled, thin, and transparent sheets that are consistent with the reported features of RGO nanosheets.[28] After *in situ* polymerization, the integrity of the nanosheets was maintained and the sharp edges of mRG nanosheets can be still observed (Fig. 3B). This result confirms that the modification step did not alter the morphology of RGO sheets.

The chemical composition of RGO nanosheets and its modified form *via in situ* approach was also investigated by X-ray photoelectron spectroscopy. The survey spectrum of RGO (Fig. 4A–C) showed main peaks of C 1s and O 1s at ∼284 and 532 eV, respectively, with C/O ratio ≈ 4. The deconvolution of C 1s and O 1s spectra displayed presence of oxygenated functional groups such as C=O and C–O, with low intensities which might
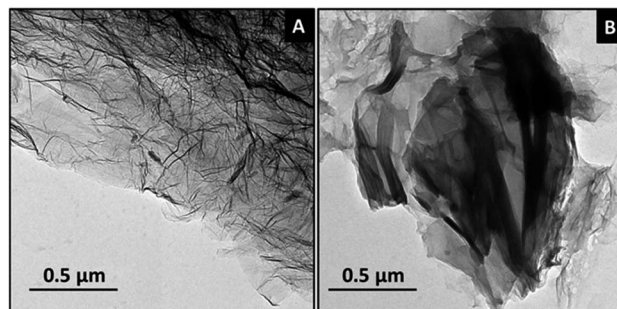

Fig. 3 TEM micrographs of [A] RGO and [B] mRG.

be attributed to the incomplete reduction due to utilization of hydrazine as reducing agent, Fig. 4B and C.[29] Moreover, the appearance of an additional peak for C–N bond at ∼400 eV after the reduction process indicates that hydrazine reduction led to restoration of sp² configuration on the basal plane of RGO and formation of aziridine and pyrazole rings which induces nitrogen doping.[30,31] The spectra of PES presented in Fig. 4D–F indicate that the prepared polymer mainly contained high percent of carbon and oxygen with a small residue of nitrogen attributed to urea derivative as a byproduct. (1) The deconvolution of C 1s band showed several peaks at 283.99, 285.46, 288.35, and 290.76 eV corresponding to C=C, C–O, C=O, and carboxylic C (HO–C=O), respectively.[32,33] (2) O 1s spectrum showed two main peaks at 531.72 and 532.69 eV corresponding to C=O and C–O, respectively.[34,35] Moreover, XPS spectra of mRG (Fig. 4G–I) showed increasing in the carbon content (82%) with C/O ratio ≈ 8 confirming presence of PES on the surface of the RGO sheets. Nevertheless, the oxygen content decreased due to presence of some residues of urea derivative byproduct, Fig. 4G. The C 1s spectrum of mRG revealed sharper and intense peaks at ∼284.01, 284.7, 285.5, 287.3, and 288.6 eV corresponding to C=C, C–C, C–O, C=O, and O–C=O, respectively, Fig. 4H. The O 1s spectrum reveals two main peaks at 530.5 and 532.47 attributed to C=O and C–O groups, respectively, in agreement with C 1s bands, Fig. 4I. Careful inspection in the spectra of RGO and comparing with the spectra of PES, one can observe a clear chemical shift in the characteristic bands of both RGO and PES bands in the produced mRG. Particularly, the carboxylic C in the PES was shifted from ∼290 eV to ∼288.6 eV. Moreover, small chemical shift for other groups emphasizes the strong linkage, *i.e.* π–π and van der Waals attraction forces, among the PES and the graphene surface which refers to a successful modification step.

Surface morphology

Morphological investigation of PCL nanocomposite films reinforced with 1 wt% of fillers compared with pristine PCL were performed using SEM. The top surface of the prepared films is shown in Fig. 5A–C. Upon addition of RGO, surface morphology exhibited a laminar like-structure Fig. 5B. However, addition of mRG to PCL matrix did not alter the surface morphology of the obtained film. This means that the surface modification of RGO with PES improved its dispersion within the matrix. On the
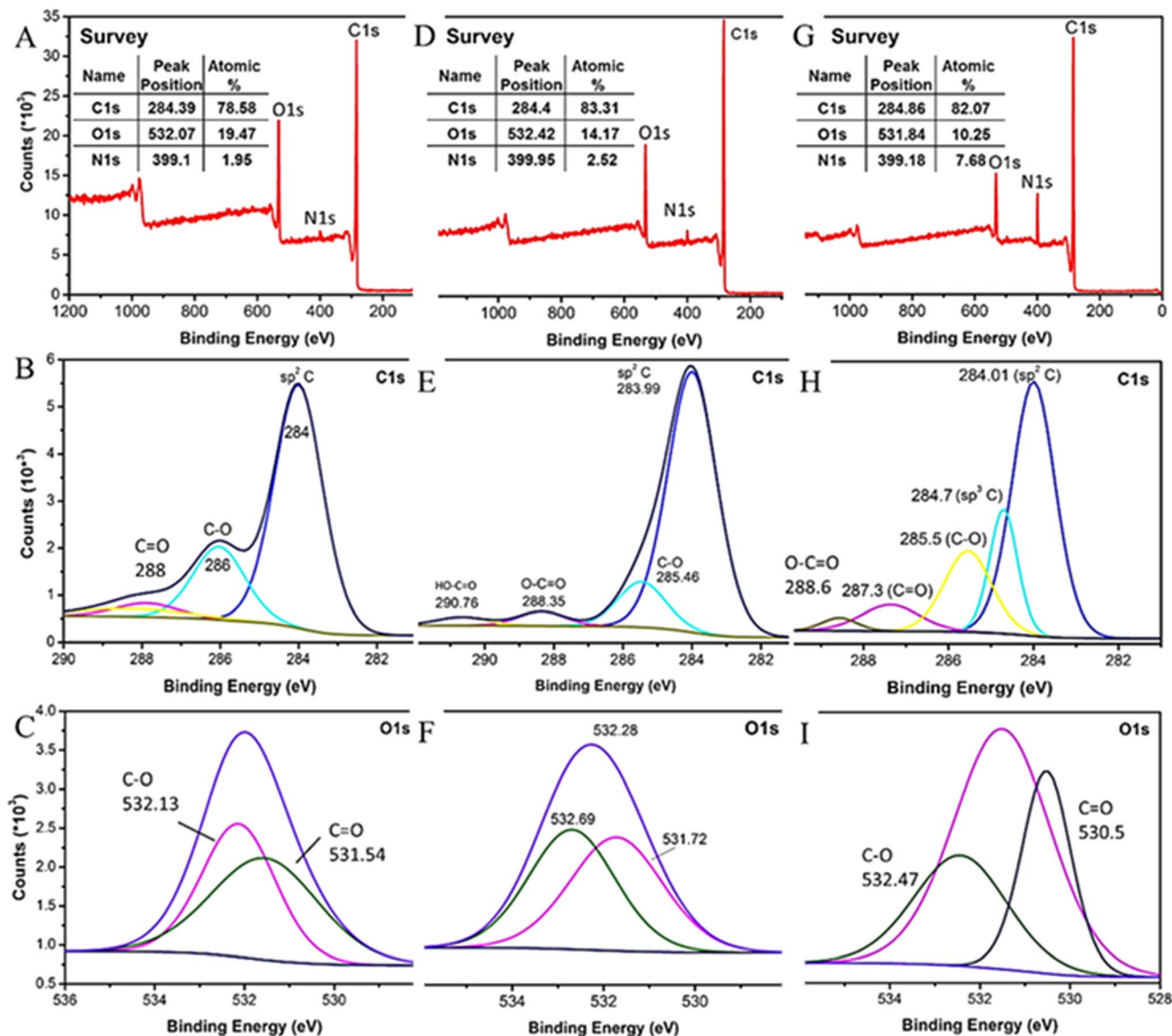
Fig. 4 XPS spectra of [A–C] reduced graphene oxide, [D–F] hyperbranched polyester, and [G–I] *in situ* modified RGO.

other hand, the cross-section images of the prepared films shown in Fig. 5D–F refer to increase of the thickness of the blank PCL film from ~140 μm to ~150 μm due to the inclusion of the modified filler while maintaining its integrity even after incorporation of modified filler.

Surface wettability

Water contact angle was measured to investigate the surface wettability of nanocomposite films containing RGO or mRG. As shown in Fig. 6, the contact angle did not show significant change by incorporation of RGO in the PCL matrix ($86 \pm 1°$). However, the contact angle of PCL/mRG film was decreased to ($79 \pm 1°$) by inclusion of mRG as illustrated in Fig. 6III. This result can be explained by the presence of high density of hydroxyl functional groups on the surface of graphene nanocomposite derived from the hyperbranched polyester chains which could improve the surface hydrophilicity of the formed

nanocomposite. As, surface tension γ_{sv} is a measure for the surface energy of the solid, it can be concluded that the film of PCL/mRG possesses the highest γ_{sv} values due to its hydrophilic character, whereas films of PCL and PCL/RGO have lower γ_{sv} *i.e.* a less hydrophilic surface.

Thermal properties

DSC thermograms were recorded to investigate the influence of nanofillers on chain mobility, crystallization and melting behaviors of PCL matrix. The DSC heating and cooling scans of the neat PCL, PCL/RGO and PCL/mRG composite films are presented in Fig. 7, and the detailed DSC results are listed in Table 1. The glass transition temperatures (T_g) of the neat PCL was equal to -66 °C, melting point (T_m) was around 63 °C and crystallization temperature (T_c) was 26 °C. These obtained results agreed with the values obtained from the literature.[25,36] The values of glass transition temperature (T_g) of neat matrix
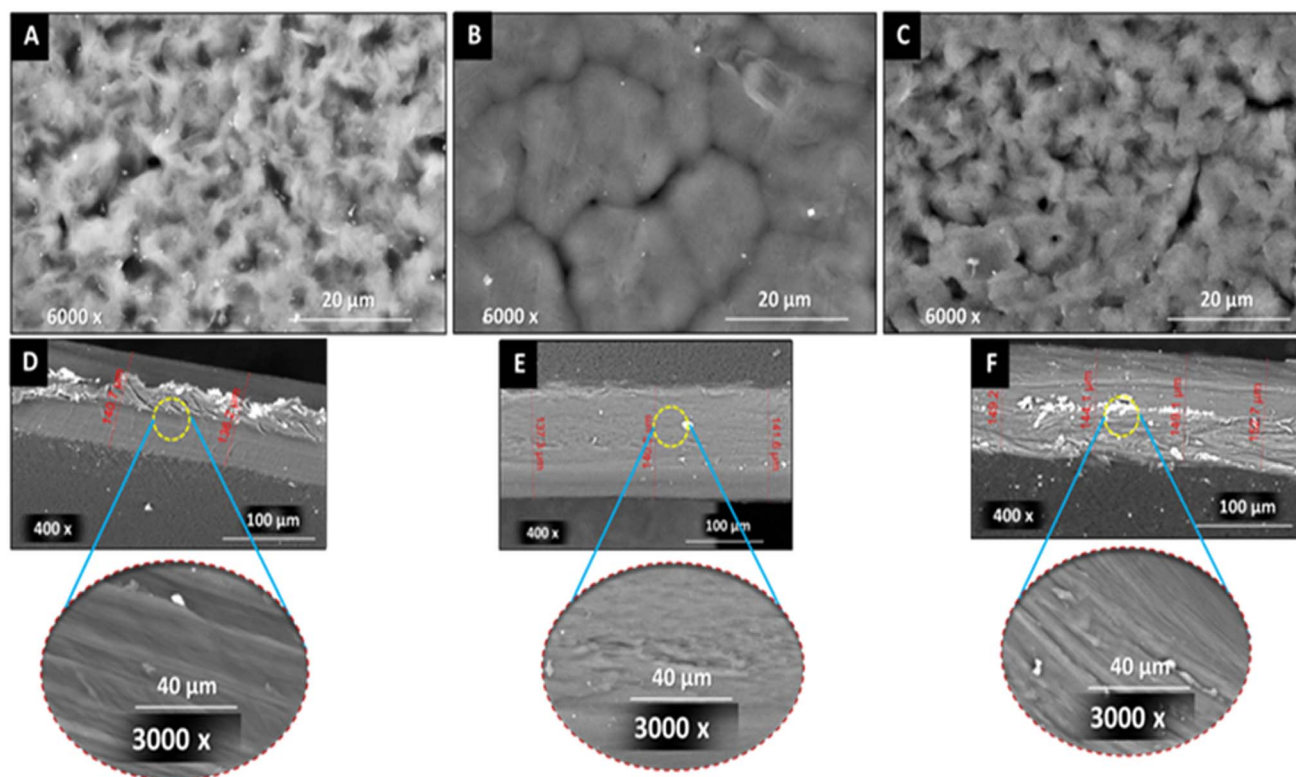
Fig. 5 SEM images of [A–C] top surfaces and [D–F] cross-sections of neat PCL film, nanocomposite films (PCL/RGO), and (PCL/mRG), respectively.
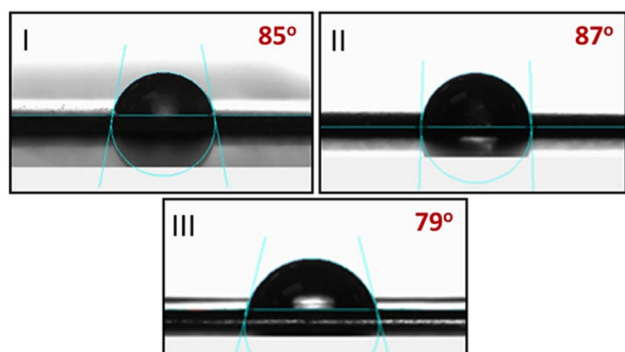

Fig. 6 Contact angle measurements of films: (I) Neat PCL, (II) PCL/RGO, and (III) PCL/mRG.

and different nanocomposites are listed in Table 1. After the incorporation of fillers, independently of its nature, no change in T_g values were observed indicating no modification of polymer chains mobility in the amorphous phase. The nanocomposite films displayed similar melting peak and similar T_m values compared to that of neat PCL ($T_m = 63 \pm 1$ °C). It can be concluded that the crystalline lamellae structure of PCL was not affected by the presence of fillers. Moreover, the calculated PCL crystallinity values for the different samples were around $72 \pm 1\%$ in consistence with values reported by Ludueña et al.[24] This indicated that addition of RGO or mRG had no effect on the crystallinity of the PCL matrix. The temperature of the maximum of the peak of crystallization (T_c) of neat PCL was
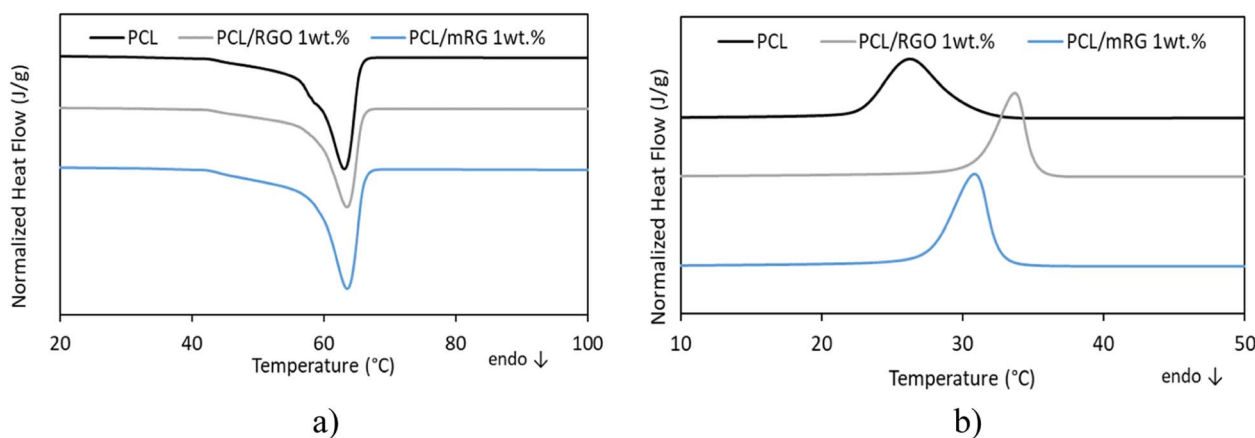

Fig. 7 DSC thermograms of (a) first heating scan (b) cooling scan of neat PCL and corresponding nanocomposites.
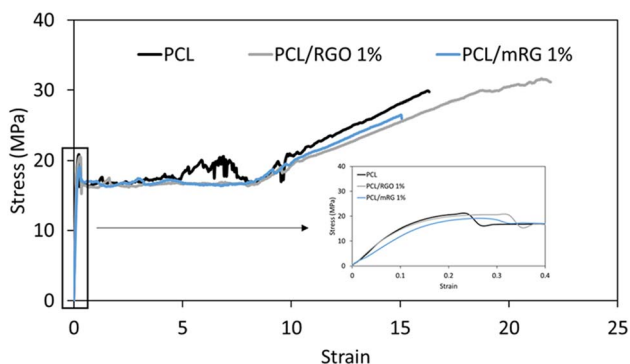
Table 1 Glass transition temperature (T_g), crystallization temperature (T_c), melting temperature (T_m), crystallinity degree (X_c) and full width at the half height maximum of the crystallization (FWHM) of neat PCL and corresponding nanocomposites

Samples	T_g (°C)	T_c (°C)	T_m (°C)	X_c (°C)	FWHM
PCL	-66 ± 1	26 ± 1	63 ± 1	71 ± 1	4.9 ± 0.1
PCL/RGO 1wt%	-66 ± 1	34 ± 1	63 ± 1	72 ± 1	3.1 ± 0.1
PCL/mRG 1wt%	-67 ± 1	31 ± 1	64 ± 1	72 ± 1	2.9 ± 0.1

measured as 26 °C. The value of T_c was consistent with those reported in the literature.[10] The addition of nanofillers into PCL matrix, independently of its nature led to an increase of the crystallization temperature (T_c) due to the nucleating effect of the nanofillers. This nucleating effect was favored in presence of RGO compared to mRG filler where T_c values were 34 °C and 31 °C respectively. Similar phenomenon has been obtained by Keramati *et al.* on polylactic acid (PLA) reinforced by graphene nanoplatelets (GNPs) and graphene nanoplatelets modified by zwitterion surfactant.[37] As the presence of the fillers induces heterogeneous nucleation, an increase of T_c can be linked to finer dispersion of the fillers. Full width at the half height maximum of the crystallization (FWHM) is another parameter that states better nucleation occurred in presence of the fillers. FWHM is proportional to the spherulite size distribution and the smaller FWHM means more nucleation and uniform crystallization.[36]

Mechanical properties

Representative stress–strain curves of neat PCL, composite films are shown in Fig. 8. All samples underwent deformation char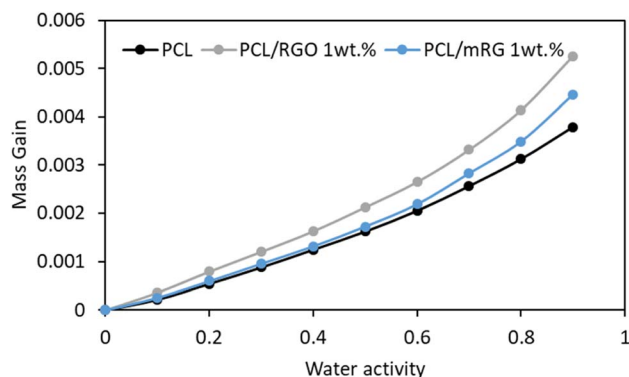acteristic of semi-crystalline and ductile polymers at room temperature exhibiting a linear increase with necking propagation and drawing followed by strain hardening effect and finally breaks at relatively long elongation.

The obtained values of neat PCL were typical to that reported in the literature.[38,39] Taking uncertainties into account, mechanical properties did not change in presence of fillers, independently of its nature as shown in Table 2.

Water sorption

Sorption isotherm curves at 25 °C were obtained by plotting the mass gain at equilibrium as a function of the water activity (a_w), Fig. 9. All isotherm curves displayed a BET III shape according to the classification of Brunauer, Emmett, and Teller.[40] A linear evolution of water uptake was observed at low water activity followed by a convex part at high activity. The increase of water uptake at high activity is usually explained by the formation of water clusters.[41–43] The obtained values of mass gain for PCL matrix were close to that obtained by Gain *et al.*[44] The presence of fillers, either RGO or mRG led to an increase of the water uptake. As the crystallinity index remained unchanged in presence of the fillers, the increase of water uptake should be explained by the sorption of water molecules by the oxygen-containing polar groups in GO. Similar results have been observed by You *et al.* on cellulose triacetate (CTA)/reduced graphene oxide nanocomposites showing an increase of the water uptake in presence of RGO.[45] The water uptake of the nanocomposites reinforced by mRG was lower compared to those obtained in presence RGO although hydrophilic nature. This result might be attributed to presence of bulky filler mRGO increased cross sectional area of the nanocomposite films as confirmed by SEM investigations, these bulk groups allowed water diffusion than sorption.

Fig. 8 Evolution of the stress strain curves for neat PCL and its nanocomposite films.

Fig. 9 Sorption isotherm curves at $T = 25$ °C of the neat PCL matrix and the different nanocomposites.

Table 2 Values of tensile modulus (E), yield stress (σ_y), yield strain (ε_y), breaking stress (σ_b) and strain at break (ε_b) determined from the stress–curves of neat PCL and nanocomposite films

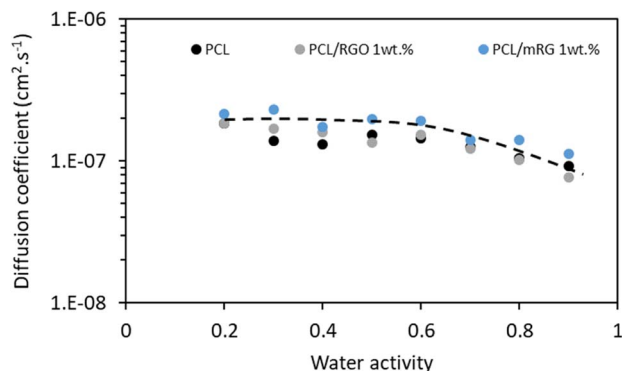| Sample	E (MPa)	σ_y (MPa)	ε_y	σ_b (MPa)	ε_b
PCL	141 ± 8	20.5 ± 0.9	0.26 ± 0.04	29.6 ± 1.4	16.4 ± 0.8
PCL/RGO 1wt%	161 ± 18	20.7 ± 0.3	0.32 ± 0.02	33.4 ± 4.5	21.2 ± 4.3
PCL/mRG 1wt%	121 ± 22	18.5 ± 0.8	0.31 ± 0.02	34.8 ± 2.0	15.1 ± 0.8

Fig. 10 Evolution of diffusion coefficient D as a function of water activity for the neat PCL matrix and the different nanocomposites.

The influence of introduced nanofillers on water sorption kinetics was also investigated. The water diffusion coefficient values (D) were plotted as a function of water activity (a_w) on a semi-logarithmic scale, Fig. 10. The obtained D values of the neat PCL agreed with those reported in the literature.[44,46] Regardless of film composition, it could be noticed that the diffusion rate was not constant over the whole range of activity, meaning that D was dependent on the number of water molecules sorbed by the films. Constant D values were recorded up to a_w of 0.7 after that decreased. This evolution of D was in accordance with the sorption isotherm curve. The constant value of D could be related to the Henry's sorption mechanism. At high water activity, the decrease of diffusion coefficient could be attributed to the water clustering phenomenon.[47,48] Considering the uncertainty, the introduction of fillers, whatever the nature did not modify diffusion of water molecules.

Gas and water permeability

The obtained values CO_2 and H_2O permeability (P_{CO_2} and P_{H_2O}) coefficients in addition to CO_2 diffusion (D_{CO_2}) coefficient are reported in Table 3. The obtained value of P_{H_2O} of neat PCL matrix at $a_w = 1$ was equal to 3430 barrer. This value was lower than that obtained by Follain *et al.* who obtained a value equal to 5959 barrer. This difference can be explained by a difference of crystallinity index.[49]

To discuss the effect of the fillers on the transport properties, the relative permeability coefficient (P_r) and the relative diffusivity coefficient (D_r) were calculated. The obtained values of P_r for CO_2 and H_2O and D_r for CO_2 are listed in Table 4. Both nanocomposite films showed similar values of P_r and D_r around 1.3 ± 0.1. Whatever the permeate molecule, the obtained values of P_r and D_r were higher than unity indicating an increase of permeability and diffusivity in presence of the fillers

Table 4 The reduction % of optical density represents the antimicrobial activity of reduced graphene oxide (RGO) and its modified form (mRG) against different microorganisms

Type	Microorganism	Reduction % of OD	
		RGO	mRG
Gram-positive	*Bacillus cereus*	82	90
	Staph. aureus	71	84
Gram-negative	*Escherichia coli*	15	20
	Pseudomonas aeruginosa	Nil	Nil
Yeast	*Candida albicans*	76	80

independently of its nature. As the crystallinity index did not change in presence of the fillers, the increase of the permeability should be explained by the presence of polar groups on the fillers. You *et al.* observed the same tendency for cellulose triacetate (CTA) reinforced by reduced graphene oxide modified with polyethylene glycol (PEG) nanocomposites.[50]

Antibacterial activity

The antimicrobial activities of RGO and mRG were investigated before incorporation in the PCL matrix. The study was assessed against two Gram-positive and two Gram-negative bacterial strains along with yeast as serious human pathogenic multidrug resistant microorganisms (see Table 4). Obviously, the recorded reduction % of the OD values relies not only on the type of filler but also on the type of bacteria since each type had a characteristic cell wall structure. The results emphasize that both RGO and mRG had significant biocidal activity against Gram-positive bacteria more than Gram-negative bacteria. Such low activity towards Gram-negative bacteria can be attributed to the double outer membrane surrounded the Gram-negative bacteria which make them less susceptible to RGO and mRG. Generally, the biocidal potential of graphene based materials is derived from its cutting sharp edges or the induction of oxidative stress. Particularly, the bacterial membrane may burst due to the sharp edges of RGO or mRG, allowing internal components to escape and ultimately resulting in cell death. Additionally, RGO may cause oxidative stress leading to oxidation of the bacterial's protein causing cell dysfunction.[20] Surface decoration of RGO with PES enhanced the antimicrobial activity of RGO since the presence of high density of surface functional group of PES facilitated the adhesion of bacteria on the surface of mRG and hence improved it biocidal activity.

The colony forming unites (CFU) of neat PCL, PCL/RGO, and PCL/mRG nanocomposite films were evaluated against *S. aureus* and *E. coli*. Here, the polymeric films were individually

Table 3 Values of CO_2 permeability and H_2O permeability and CO_2 diffusion coefficients for the PCL and its nanocomposite films

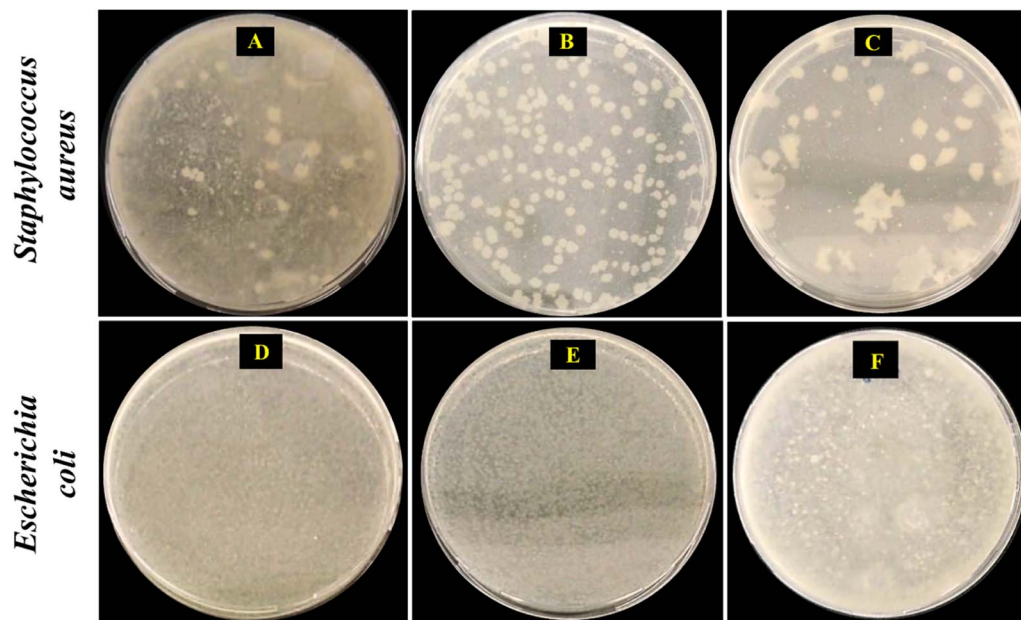| Sample	P_{H_2O} (barrer)	$P_{r(H_2O)}$	P_{CO_2} (barrer)	$P_{r(CO_2)}$	D_{CO_2} (10^{-8} cm^2 s^{-1})	$D_{r(CO_2)}$
PCL	3430 ± 250		4.37 ± 0.24		2.60 ± 0.12	
PCL/RGO	4190 ± 290	1.22 ± 0.19	6.20 ± 0.42	1.42 ± 0.18	3.20 ± 0.15	1.23 ± 0.18
PCL/mRG	4150 ± 220	1.21 ± 0.18	6.17 ± 0.4	1.41 ± 0.18	3.60 ± 0.15	1.38 ± 0.20

Fig. 11 Digital images of viable bacterial colonies of *S. aureus* [A–C] and *E. coli* strains [D–F] against neat PCL, PCL/RGO, and PCL/mRG, respectively, after 24 h of incubation and reinoculated on agar plates.
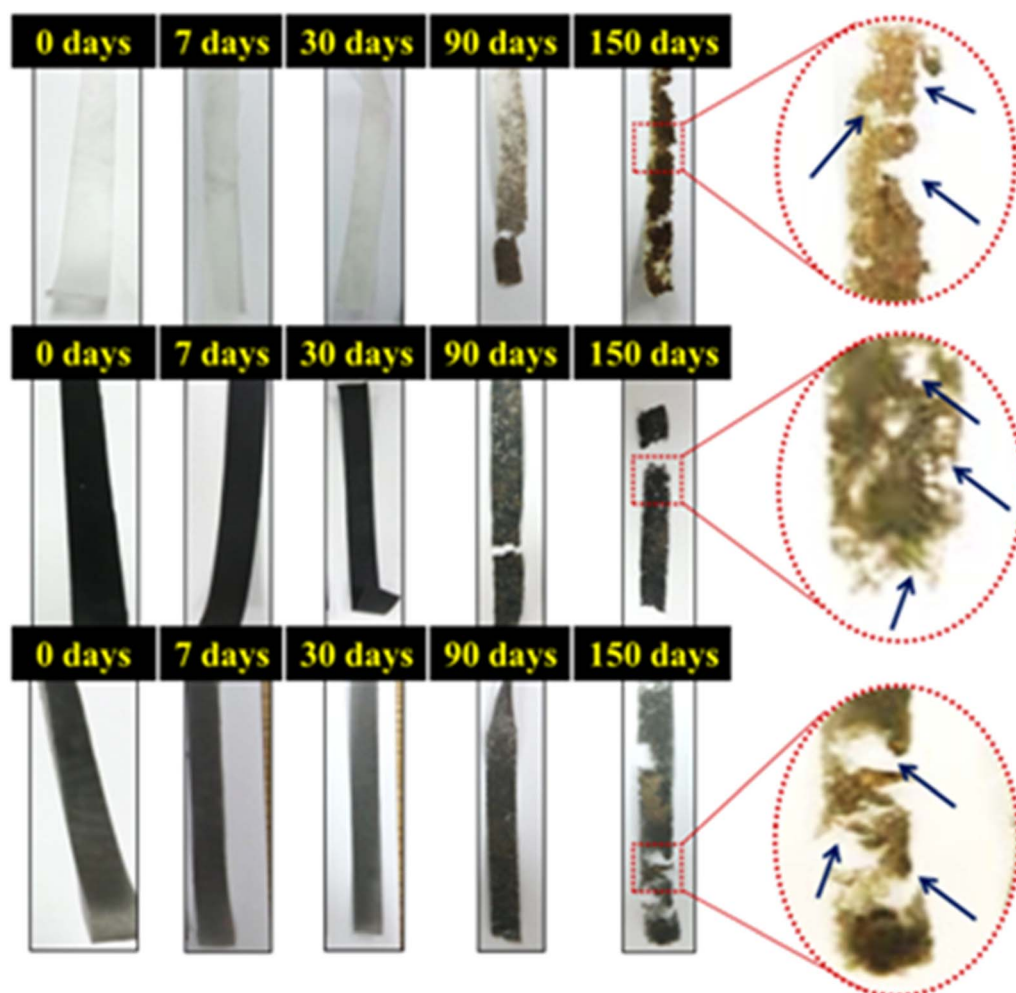

Fig. 12 Set of visual pictures for films strips before and after biodegradation over five months. Top images are neat PCL films; middle and bottom are PCL/RGO and PCL/mRG nanocomposite films, respectively.
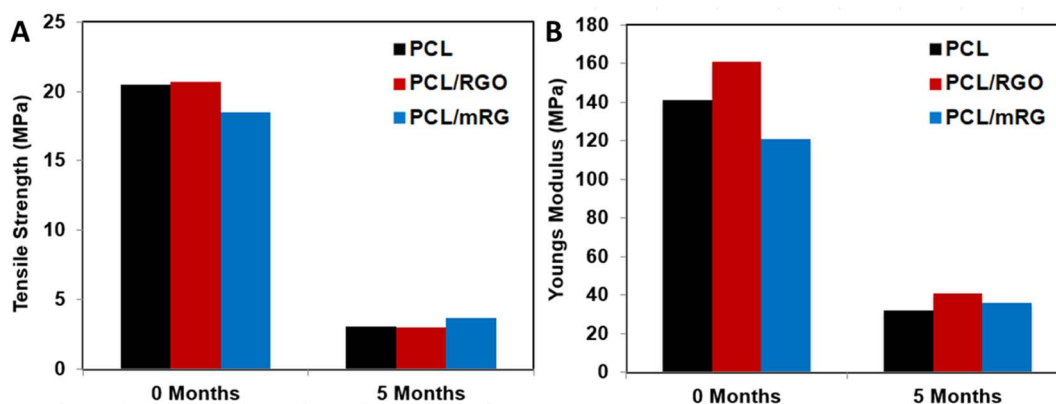
Fig. 13 Mechanical properties of PCL and its nanocomposite films. (A) Tensile stress and (B) Young modulus at 0 and 5 months of degradation in soil.

incubated in bacterial suspensions for 24 h. The surrounding bacteria was diluted and reinoculated on agar plates to calculate the colony forming unites (CFU) of the remaining alive bacteria as shown in Fig. 11A, huge numbers of viable bacterial colonies was observed which displayed that PCL had no antimicrobial activity like common polyesters (10^8 CFU mL^{-1}).[10] Fig. 11B and C obviously displayed that the number of colonies was reduced to large extent in case of PCL/RGO (229×10^4 CFU mL^{-1}) and it was further decreased in case of PCL/mRG (79×10^4 CFU mL^{-1}). In consistence with the above mentioned antimicrobial results of fillers, the prepared films had no activity against Gram-negative bacteria (Fig. 11D–F). Indeed, the results confirmed that the prepared PCL film incorporated with modified graphene acquired antimicrobial property selectively toward Gram-positive bacteria.

Ability for biodegradation

The biodegradability test was performed for neat PCL film, PCL/RGO and PCL/mRG composite films over five months in soil (Fig. 12). The results emphasized that the film degradation became pronounced after three months for all samples. However, the films had lost most of their mechanical properties after five months (Fig. 13). This indicated that the incorporation of RGO or mRG mostly did not alter the soil biodegradation of PCL matrix. Indeed, the weight loss was difficult to be measured due to filling of the formed cracks and pores with the soil dust which was very hard to get ride.

Conclusion

The surface of reduced graphene oxide (RGO) was modified with hyperbranched polyester (PES) to form modified filler (mRG) in order to facilitate its dispersion (1 wt%) in PCL matrix. Surface modification of RGO nanosheets was confirmed by FTIR, Raman and XPS spectroscopy. Morphology and hydrophilicity of nanocomposites were also investigated. A rather good dispersion of fillers within the matrix was observed and was favored in presence of mRG. Contact angle measurements displayed a slight hydrophilicity of the nanocomposite film owing

to the hydroxyl terminals of PES. The influence of the fillers on the thermal, mechanical and gas and water transport properties were evaluated. Study of thermal properties revealed that addition of RGO or mRG had no effect on the crystallinity index and the glass transition temperature values of the PCL matrix. The mechanical properties of the PCL did not change upon addition of either filler too. However, inclusion of fillers increased permeability and diffusivity, regardless of their composition. In addition, antimicrobial and biodegradability studies were carried out. The nanocomposites displayed significant antibacterial potential against Gram-positive however, Gram-negative bacteria was less susceptible. The biodegradability test revealed that for all samples, film degradation became noticeable after three months.

Data availability

All data generated or analyzed during this study are included in this article.

Author contributions

Ahamed Ghanem participated in samples preparation, characterization and data analysis M. Yassin participated in the chemical & morphological characterizations and data analysis Raphael Cosquer performed the mechanical testing while Fabrice Gouanvé carried out barrier properties investigations and analyzed the data. Eliane Espuche and Mona Abdel Rehim have contributed in designing the study and revising the manuscript. All authors are contributed equally in interpreting the results and writing the manuscript.

Conflicts of interest

The authors declare that no conflicts of interest exist.

Acknowledgements

Research and Technology (ASRT) is deeply acknowledged. This work is dedicated to the soul of Prof. A. Rabie.

References

1 M. H. Abdel Rehim, Bio-Based Polyesters for Ecofriendly Packaging Materials, *Egypt. J. Chem.*, 2022, **65**(13B), 1145–1153, DOI: **10.21608/ejchem.2022.156185.6768**.

2 M. Naguib and M. A. Yassin, Polymeric Antioxidant via ROMP of Bioderived Tricyclic Oxanorbornene Based on Vanillin and Furfurylamine, *ACS Appl. Polym. Mater.*, 2022, **4**(3), 2181–2188, DOI: **10.1021/acsapm.2c00158**.

3 M. Naguib, M. A. Yassin and M. A. Rehim, Antimicrobial Polyurethane Films Based on Quaternary Ammonium Salts Functionalized Soybean Oil, *Macromol. Chem. Phys.*, 2023, **224**(1), 2200231, DOI: **10.1002/macp.202200231**.

4 A. Duda, A. Kowalski, S. Penczek, H. Uyama and S. Kobayashi, Kinetics of the Ring-Opening Polymerization of 6-, 7-, 9-, 12-, 13-, 16-, and 17-Membered Lactones. Comparison of Chemical and Enzymatic Polymerizations, *Macromolecules*, 2002, **35**, 4266–4270, DOI: **10.1021/ma012207y**.

5 S. Khalid, L. Yu, M. Feng, L. Meng, Y. Bai, A. Ali, H. Liu and L. Chen, Development and Characterization of Biodegradable Antimicrobial Packaging Films Based on Polycaprolactone, Starch and Pomegranate Rind Hybrids, *Food Packag. Shelf Life*, 2018, **18**, 71–79, DOI: **10.1016/j.fpsl.2018.08.008**.

6 A. K. Sundramoorthy, T. H. Vignesh Kumar and S. Gunasekaran, Graphene-Based Nanosensors and Smart Food Packaging Systems for Food Safety and Quality Monitoring, in *Graphene Bioelectronics*, Elsevier, 2018, pp. 267–306, ISBN 978-0-12-813349-1.

7 A. F. Ghanem, A. M. Youssef and M. H. Abdel Rehim, Hydrophobically Modified Graphene Oxide as a Barrier and Antibacterial Agent for Polystyrene Packaging, *J. Mater. Sci.*, 2020, **55**, 4685–4700, DOI: **10.1007/s10853-019-04333-7**.

8 Q. Xu, Y. Gong, Y. Fang, G. Jiang, Y. Wang, X. Sun and R. Wang, Straightforward Synthesis of Hyperbranched Polymer/Graphene Nanocomposites from Graphite Oxide via in Situ Grafting from Approach, *Bull. Mater. Sci.*, 2012, **35**, 795–800, DOI: **10.1007/s12034-012-0378-3**.

9 J. Liu, W. Yang, L. Tao, D. Li, C. Boyer and T. P. Davis, Thermosensitive Graphene Nanocomposites Formed Using Pyrene-Terminal Polymers Made by RAFT Polymerization: Thermosensitive Graphene Nanocomposites, *J. Polym. Sci., Part A: Polym. Chem.*, 2010, **48**, 425–433, DOI: **10.1002/pola.23802**.

10 T. Das, S. Sengupta, A. Jana, A. Pal, I. Roy, S. Sardar, N. R. Saha, S. Ghosh and A. Bandyopadhyay, Graphene Oxide Grafted Hyperbranched Poly (Vinyl Imidazole) with Ionic Liquid Components as a Potential Carbon Dioxide Scrubber, *React. Funct. Polym.*, 2020, **146**, 104432, DOI: **10.1016/j.reactfunctpolym.2019.104432**.

11 Y. Liu, J. Zheng, X. Zhang, Y. Du, G. Yu, K. Li, Y. Jia and Y. Zhang, Hyperbranched Polyamide Modified Graphene Oxide-Reinforced Polyurethane Nanocomposites with Enhanced Mechanical Properties, *RSC Adv.*, 2021, **11**, 14484–14494, DOI: **10.1039/D1RA00654A**.

12 Z. Hao, L. Li, B. Yang, X. Sheng, X. Liao, L. He and P. Liu, Influences of Hyperbranched Polyester Modification on the Crystallization Kinetics of Isotactic Polypropylene/Graphene Oxide Composites, *Polymers*, 2019, **11**, 433, DOI: **10.3390/polym11030433**.

13 T. Guo, H. Li, X. Ma, L. Shi, W. Wang, W. Zhang and L. Li, Hyperbranched Polyester Modified Graphene Oxide on Anti-Corrosion Performance of Epoxy Composite Coatings for Electric Power System, *Plast., Rubber Compos.*, 2020, **49**, 245–253, DOI: **10.1080/14658011.2020.1735180**.

14 C. Wan and B. Chen, Poly(ε-caprolactone)/graphene oxide biocomposites: Mechanical properties and bioactivity, *Biomed. Mater.*, 2011, **6**, 1–8, DOI: **10.1088/1748-6041/6/5/055010**.

15 M. Bagheri and A. Mahmoodzadeh, Polycaprolactone/graphene nanocomposites: Synthesis, characterization and mechanical properties of electrospun nanofibers, *J. Inorg. Organomet. Polym. Mater.*, 2020, **30**, 1566–1577.

16 G. S. Wang, Z. Y. Wei, L. Sang, G. Y. Chen, W. X. Zhang, X. F. Dong and M. Qi, Morphology, crystallization and mechanical properties of poly(ε-caprolactone)/graphene oxide nanocomposites, *Chin. J. Polym. Sci.*, 2013, **31**, 1148–1160, DOI: **10.1007/s10118-013-1278-8**.

17 J. Zhang and Z. Qiu, Morphology, crystallization behavior, and dynamic mechanical properties of biodegradable poly(ε-caprolactone)/thermally reduced graphene nanocomposites, *Ind. Eng. Chem. Res.*, 2011, **50**, 13885–13891, DOI: **10.1021/ie202132m**.

18 S. Sayyar, E. Murray, B. C. Thompson, S. Gambhir, D. L. Officer and G. G. Wallace, Covalently Linked Biocompatible Graphene/Polycaprolactone Composites for Tissue Engineering, *Carbon*, 2013, **52**, 296–304, DOI: **10.1016/j.carbon.2012.09.031**.

19 C.-Y. Lee, S. Sayyar, P. J. Molino and G. G. Wallace, A Robust 3D Printed Multilayer Conductive Graphene/Polycaprolactone Composite Electrode, *Mater. Chem. Front.*, 2020, **4**, 1664–1670, DOI: **10.1039/C9QM00780F**.

20 A. F. Ghanem, M. A. Yassin, A. M. Rabie, F. Gouanvé, E. Espuche and M. H. Abdel Rehim, Investigation of Water Sorption, Gas Barrier and Antimicrobial Properties of Polycaprolactone Films Contain Modified Graphene, *J. Mater. Sci.*, 2021, **56**, 497–512, DOI: **10.1007/s10853-020-05329-4**.

21 S. Sánchez-González, N. Diban and A. Urtiaga, Hydrolytic Degradation and Mechanical Stability of Poly(ε-Caprolactone)/Reduced Graphene Oxide Membranes as Scaffolds for In Vitro Neural Tissue Regeneration, *Membranes*, 2018, **8**, 12, DOI: **10.3390/membranes8010012**.

22 W. S. Hummers and R. E. Offeman, Preparation of Graphitic Oxide, *J. Am. Chem. Soc.*, 1958, **80**, 1339, DOI: **10.1021/ja01539a017**.

23 A. F. Ghanem, A. A. Badawy, N. Ismail, Z. Rayn Tian, M. H. Abdel Rehim and A. Rabia, Photocatalytic Activity of Hyperbranched Polyester/TiO$_2$ Nanocomposites, *Appl.*

Catal., *A*, 2014, **472**, 191–197, DOI: 10.1016/j.apcata.2013.12.023.

24 L. N. Ludueña, J. M. Kenny, A. Vázquez and V. A. Alvarez, Effect of Clay Organic Modifier on the Final Performance of PCL/Clay Nanocomposites, *Mater. Sci. Eng., A*, 2011, **529**, 215–223, DOI: 10.1016/j.msea.2011.09.020.

25 C. G. Pitt, F. I. Chasalow, Y. M. Hibionada, D. M. Klimas and A. Schindler, Aliphatic Polyesters. I. The Degradation of Poly(ε-Caprolactone) in Vivo, *J. Appl. Polym. Sci.*, 1981, **26**, 3779–3787, DOI: 10.1002/app.1981.070261124.

26 A. B. Abou Hammad, M. E. Abd El-Aziz, M. S. Hasanin and S. Kamel, A Novel Electromagnetic Biodegradable Nanocomposite Based on Cellulose, Polyaniline, and Cobalt Ferrite Nanoparticles, *Carbohydr. Polym.*, 2019, **216**, 54–62, DOI: 10.1016/j.carbpol.2019.03.038.

27 M. J. Deka and D. Chowdhury, Tuning Electrical Properties of Graphene with Different π-Stacking Organic Molecules, *J. Phys. Chem. C*, 2016, **120**, 4121–4129, DOI: 10.1021/acs.jpcc.5b12403.

28 B. Subramanya and D. K. Bhat, Novel One-Pot Green Synthesis of Graphene in Aqueous Medium under Microwave Irradiation Using a Regenerative Catalyst and the Study of Its Electrochemical Properties, *New J. Chem.*, 2015, **39**, 420–430, DOI: 10.1039/C4NJ01359J.

29 Y.-E. Shin, Y. J. Sa, S. Park, J. Lee, K.-H. Shin, S. H. Joo and H. Ko, An Ice-Templated, PH-Tunable Self-Assembly Route to Hierarchically Porous Graphene Nanoscroll Networks, *Nanoscale*, 2014, **6**, 9734–9741, DOI: 10.1039/C4NR01988A.

30 S. Park, Y. Hu, J. O. Hwang, E.-S. Lee, L. B. Casabianca, W. Cai, J. R. Potts, H.-W. Ha, S. Chen, J. Oh, *et al.*, Chemical Structures of Hydrazine-Treated Graphene Oxide and Generation of Aromatic Nitrogen Doping, *Nat. Commun.*, 2012, **3**, 638, DOI: 10.1038/ncomms1643.

31 K. Dave, K. H. Park and M. Dhayal, Two-Step Process for Programmable Removal of Oxygen Functionalities of Graphene Oxide: Functional, Structural and Electrical Characteristics, *RSC Adv.*, 2015, **5**, 95657–95665, DOI: 10.1039/C5RA18880F.

32 M. Ashraf, P. Champagne, C. Campagne, A. Perwuelz, F. Dumont and A. Leriche, Study the Multi Self-Cleaning Characteristics of ZnO Nanorods Functionalized Polyester Fabric, *J. Ind. Text.*, 2016, **45**, 1440–1456, DOI: 10.1177/1528083714562086.

33 S. Pletincx, K. Marcoen, L. Trotochaud, L.-L. Fockaert, J. M. C. Mol, A. R. Head, O. Karslioğlu, H. Bluhm, H. Terryn and T. Hauffman, Unravelling the Chemical Influence of Water on the PMMA/Aluminum Oxide Hybrid Interface In Situ, *Sci. Rep.*, 2017, **7**, 13341, DOI: 10.1038/s41598-017-13549-z.

34 L. Li, X. Liao, X. Sheng, Z. Hao, L. He, P. Liu, H. Quan and Y. Zhang, Effect of Structure Regulation of Hyper-Branched Polyester Modified Carbon Nanotubes on Toughening Performance of Epoxy/Carbon Nanotube Nanocomposites, *RSC Adv.*, 2019, **9**, 12864–12876, DOI: 10.1039/C9RA01550G.

35 T. Shen, Y. Liu, Y. Zhu, D.-Q. Yang and E. Sacher, Improved Adhesion of Ag NPs to the Polyethylene Terephthalate Surface via Atmospheric Plasma Treatment and Surface Functionalization, *Appl. Surf. Sci.*, 2017, **411**, 411–418, DOI: 10.1016/j.apsusc.2017.03.149.

36 L. Ludueña, A. Vázquez and V. Alvarez, Viscoelastic Behavior of Polycaprolactone/Clay Nanocomposites, *J. Compos. Mater.*, 2012, **46**, 677–689, DOI: 10.1177/0021998311410476.

37 M. Keramati, I. Ghasemi, M. Karrabi, H. Azizi and M. Sabzi, Incorporation of Surface Modified Graphene Nanoplatelets for Development of Shape Memory PLA Nanocomposite, *Fibers Polym.*, 2016, **17**, 1062–1068, DOI: 10.1007/s12221-016-6329-7.

38 L. Ludueña, J. Kenny, A. Vázquez and V. Alvarez, Effect of Extrusion Conditions and Post-Extrusion Techniques on the Morphology and Thermal/Mechanical Properties of Polycaprolactone/Clay Nanocomposites, *J. Compos. Mater.*, 2014, **48**, 2059–2070, DOI: 10.1177/0021998313494103.

39 A. S. Hadj-Hamou, F. Metref and F. Yahiaoui, Thermal Stability and Decomposition Kinetic Studies of Antimicrobial PCL/Nanoclay Packaging Films, *Polym. Bull.*, 2017, **74**, 3833–3853, DOI: 10.1007/s00289-017-1929-y.

40 S. Brunauer and P. H. Emmett, The Use of Low Temperature van Der Waals Adsorption Isotherms in Determining the Surface Areas of Various Adsorbents, *J. Am. Chem. Soc.*, 1937, **59**, 2682–2689, DOI: 10.1021/ja01291a060.

41 A. Blanchard, F. Gouanvé and E. Espuche, Effect of Humidity on Mechanical, Thermal and Barrier Properties of EVOH Films, *J. Membr. Sci.*, 2017, **540**, 1–9, DOI: 10.1016/j.memsci.2017.06.031.

42 P. Cheviron, F. Gouanvé and E. Espuche, Preparation, Characterization and Barrier Properties of Silver/Montmorillonite/Starch Nanocomposite Films, *J. Membr. Sci.*, 2016, **497**, 162–171, DOI: 10.1016/j.memsci.2015.09.039.

43 R. Cosquer, S. Pruvost and F. Gouanvé, Improvement of Barrier Properties of Biodegradable Polybutylene Succinate/Graphene Nanoplatelets Nanocomposites Prepared by Melt Process, *Membranes*, 2021, **11**, 151, DOI: 10.3390/membranes11020151.

44 O. Gain, E. Espuche, E. Pollet, M. Alexandre and Ph. Dubois, Gas Barrier Properties of Poly(ε-Caprolactone)/Clay Nanocomposites: Influence of the Morphology and Polymer/Clay Interactions, *J. Polym. Sci., Part B: Polym. Phys.*, 2005, **43**, 205–214, DOI: 10.1002/polb.20316.

45 M. You, B. Wang, P. Singh and J. Meng, Water and Salt Transport Properties of the Cellulose Triacetate/Reduced Graphene Oxide Nanocomposite Membranes, *Polymer*, 2020, **210**, 122976, DOI: 10.1016/j.polymer.2020.122976.

46 G. Gorrasi, M. Tortora, V. Vittoria, E. Pollet, B. Lepoittevin, M. Alexandre and P. Dubois, Vapor Barrier Properties of Polycaprolactone Montmorillonite Nanocomposites: Effect of Clay Dispersion, *Polymer*, 2003, **44**, 2271–2279, DOI: 10.1016/S0032-3861(03)00108-3.

47 P. E. Rouse, Diffusion of Vapors in Films, *J. Am. Chem. Soc.*, 1947, **69**, 1068–1073, DOI: 10.1021/ja01197a029.

48 R. Cosquer, S. Pruvost and F. Gouanvé, Effect of Temperature and Humidity on the Water and Dioxygen Transport Properties of Polybutylene Succinate/Graphene Nanoplatelets Nanocomposite Films, *Membranes*, 2022, **12**, 721, DOI: 10.3390/membranes12070721.

49 N. Follain, S. Belbekhouche, J. Bras, G. Siqueira, S. Marais and A. Dufresne, Water Transport Properties of Bio-Nanocomposites Reinforced by Luffa Cylindrica Cellulose Nanocrystals, *J. Membr. Sci.*, 2013, **427**, 218–229, DOI: **10.1016/j.memsci.2012.09.048**.

50 M. You, D. Yao, F. Xu, C. Zhang and J. Meng, Surface Modification of RGO with PEG for the Improvement of Water/Salt Selectivity of CTA/RGO Nanocomposites for Desalination Membrane Applications, *Polymer*, 2022, **256**, 125228, DOI: **10.1016/j.polymer.2022.125228**.